JOURNAL OF GUIDANCE, CONTROL, AND DYNAMICS
Vol. 18, No. 2, March–April 1995

Analytically and Numerically Derived H_∞ Controller Designs for Hubble Space Telescope

R. Dennis Irwin,* Russell D. Glenn,† W. Garth Frazier,‡ and Douglas A. Lawrence§
Ohio University, Athens, Ohio 45701
and
Randolph F. Follett¶
Mississippi State University, Mississippi State, Mississippi 39762

Efforts in designing controllers that improve the performance of the Hubble Space Telescope pointing control system in the presence of thermally induced solar array vibration disturbances are presented. The controller redesign provides an excellent opportunity to apply state-of-the-art design techniques to a realistic multi-input, multi-output plant. Available plant models are examined with regard to their utility for controller design and simulation. The performance of existing flight controllers is studied, yielding a redesign philosophy of providing high, broadband controller gain in the frequency ranges where significant disturbance power exists to achieve improved disturbance attenuation. Under this philosophy, a controller is obtained using a standard H_∞ design approach and an alternative design is accomplished through a numerical search-based algorithm. The new controllers are compared to an existing flight-tested controller via frequency response analysis and through a time-domain simulation that includes vehicle torque limits and an emulation of fixed-point arithmetic effects.

Nomenclature

G_{delay} = computational delay of control computer
G_{design} = free stage of controller
G_{diff} = digital differentiators
G_{fix} = fixed stage of controller
G_{HST} = discretized model of the Hubble Space Telescope
G_{Iv} = inertia matrix
T_d = torque disturbances used to model impact of SA vibration
$\Delta\theta_{\text{cmd}}$ = commanded change in attitude (commanded rate)
θ_{meas} = measured attitude

Introduction

THE pointing control system (PCS) onboard the Hubble Space Telescope (HST) is required to maintain line-of-sight (LOS) pointing error below 0.007 arc-s for observations lasting as long as 24 h. Since deployment, an unanticipated disturbance source has resulted in LOS jitter far exceeding this requirement. Detailed analysis has indicated that this disturbance is most likely due to thermally induced in-plane and out-of-plane flexing of the solar arrays (SAs) at frequencies of roughly 0.6 and 0.11 Hz, respectively. NASA efforts to redesign the HST PCS have led to the solar array gain augmentation (SAGA-II) controller, which yields significant, yet insufficient, pointing error attenuation.

Efforts in applying multi-input, multi-output (MIMO) analysis and design techniques to the PCS redesign problem are presented. In particular, the notion of singular-value frequency response (i.e., H_∞ specifications) is used extensively in formulating performance specifications and performing stability analyses for coupled MIMO systems such as the HST. These H_∞ specifications are used to design new controllers that yield improved performance over the existing flight-tested controllers.

Received Oct. 26, 1993; revision received Feb. 17, 1994; accepted for publication Sept. 22, 1994.

*Associate Professor, Department of Electrical and Computer Engineering, Stocker Center. Member AIAA.
†Stocker Fellow and Research Associate, Department of Electrical and Computer Engineering, Stocker Center.
‡Research Associate, Department of Electrical and Computer Engineering, Stocker Center.
§Assistant Professor, Department of Electrical and Computer Engineering, Stocker Center. Member AIAA.
¶Assistant Professor, Department of Electrical and Computer Engineering, P.O. Drawer EE. Member AIAA.

Hubble Space Telescope Control Redesign Problem Definition

A pictorial representation of the HST is given by Fig. 1. In this paper the axis labeled V_1 is referred to as the roll axis, V_2 is the pitch axis, and V_3 is the yaw axis. Previous NASA/Lockheed redesigns dealt only with the gyro/hold portion of the PCS; therefore only that portion is considered in the redesign. A simplified block diagram of the gyro/hold portion of the PCS with the SAGA-II controller is given in Fig. 2. It is clear that these loops form a three-input, three-output 40-Hz sampled-data system with an 8-ms computational delay. The blocks labeled $T_{W/V}$ and $T_{V/G}$ are, respectively, the body coordinate to reaction wheel assembly (RWA) transformation matrix and the rate gyro assembly (RGA) to body coordinate transformation matrix. The block labeled G_p represents the HST plant transfer function matrix, G_A is the gain augmentation filter component of the SAGA-II controller, I_V is the HST inertia matrix, and PID is a proportional-integral-derivative (PID) controller. The predominant SA disturbance effects with the original PID controller are at roughly 0.1 and 0.6 Hz.[1] These are thought to be primarily due to thermally induced out-of-plane and in-plane SA bending modes, respectively.

The SAGA-II controller implements gain peaks at the frequencies of the predominant disturbances, providing closed-loop gain notches at these frequencies. The preliminary flight data reported in Ref. 1 verify that the SAGA-II controller has achieved significant attenuation of the 0.1- and 0.6-Hz disturbances. However, the LOS power spectral density (PSD) estimates presented in Ref. 1 for the SAGA-II controller show significant disturbance power is present in the frequencies surrounding the notches.

The design approach reported here is primarily that of attempting to reduce the effects of low-frequency disturbances by providing high, broadband controller gain in the frequency ranges where the disturbances are known to exist. The resulting increased loop gain will provide broadband attenuation of low-frequency disturbances.

For the present redesign effort the following are goals:

1) Maintain the per-axis LOS jitter below 0.005 arc-s throughout a 500-s simulation that includes a day-to-night terminator crossing.

2) Maintain system type at three in each axis in order to provide rejection of low-frequency gravity gradient and aerodynamic

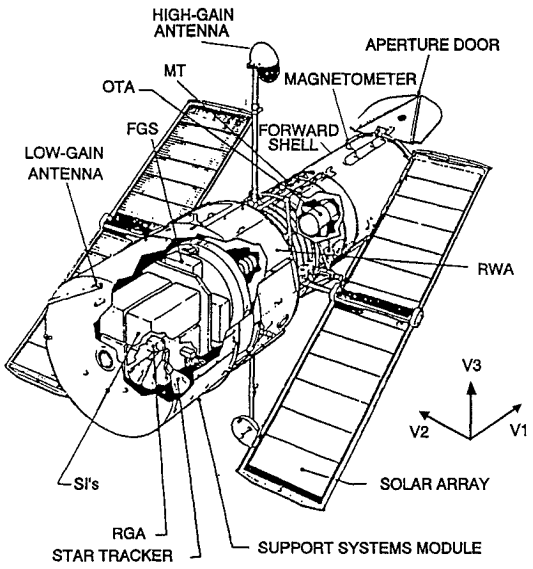

Fig. 1 Hubble Space Telescope.

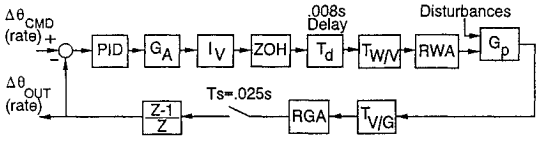

Fig. 2 Simplified PCS gyro hold block diagram.

disturbance torques and also to maintain the gyro hold controller interface to the outer attitude loops.

3) Maintain the jitter specification of requirement 1 in the face of 0.8 N-m torque limits in RWA coordinates.

4) Maintain the jitter specification when implemented in 24-bit fixed-point arithmetic using 13 bits to the right of the radix point.

Modeling Issues

Several sets of HST models were provided by NASA in support of the PCS redesign effort. Reference 1 contains a set of prelaunch and postlaunch modal gain coefficients for composite single-input, single-output (SISO) modal models. Since the intent of this effort is to apply MIMO design techniques to the HST, no designs were attempted based on the SISO models.

Four continuous-time HST models derived from the TREETOPS computer program at NASA Marshall Space Flight Center were also provided. The TREETOPS models were originally developed to provide a simulation model for independent verification of HST controller designs. The four models correspond to the 0 deg, 45 deg, 90 deg, and 105 deg SA orientations and are 118th order. The inputs are the control torques in the three vehicle axes and various disturbance torques fabricated for other purposes when the models were generated. The outputs are the angular rates and positions in the three vehicle axes. A computer file provided by NASA discretizes the realization and incorporates the computational delay as a first-degree Padé approximation.

Since the controller can directly affect only the torque inputs and the PCS loop is a rate control loop, only the portion of the model characterizing the effects of the control inputs on the vehicle rate outputs is required for design and simulation of PCS controllers. The realization corresponding to this portion of the model is of very high dimension, since it contains all the states resulting from the presence of the disturbance inputs. Schur model reduction and balanced model reduction techniques were applied to the TREETOPS models in an attempt to obtain minimal reduced-order plant models. Considerable numerical difficulties were encountered, with the result that no stabilizable and detectable reduced-order models were obtained. This has been the case whenever the authors have attempted to use modern reduction techniques and software with high-order (>80) models of nonmodal type.[2] Since no stabilizable and detectable TREETOPS-based plant models were obtainable, it was decided that the TREETOPS models were unsuitable for controller design with H_∞ techniques. However, a numerical technique that performs designs based on frequency responses, rather than the models themselves, was successfully used in conjunction with the full-order TREETOPS models. The results are presented subsequently.

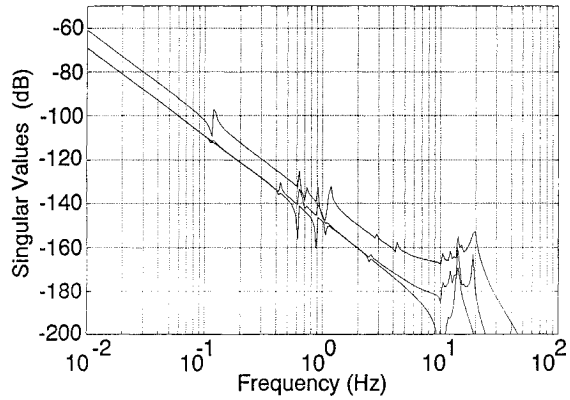

Fig. 3 Singular-value response of continuous MIMO modal model.

NASA provided a third set of models in the form of prelaunch modal gain product matrices for 0 deg, 45 deg, and 90 deg SA orientations. A continuous-time 90 deg SA orientation MIMO modal model was built by using the modal gain product matrices from Ref. 3 that correspond to the frequencies of the 23 flexible modes included in the composite SISO modal model. Using this approach and including the rigid-body modes yields a 52nd-order MIMO modal model that is fully state observable and fully state controllable. Figure 3 displays the singular-value frequency response of this model. Discretizing this model, incorporating the computational delay as a first-degree Padé approximation, and converting to the w plane result in a model that is minimal and thus suitable for use with H_∞ design techniques. Hereafter, this model is referred to as the MIMO modal plant model.

Simulation

Two simulations of the HST PCS were provided for the redesign effort: a linear simulation and a nonlinear simulation that includes torque limits and a fixed-point arithmetic implementation. Both simulations are based on a method whereby actual recorded in-flight vehicle rate data are "played back" through the simulation, yielding the vehicle rate data that would result if the controller being simulated had been in the HST rather than the controller in place when the flight data were recorded. Reference 1 presents a SISO derivation of the simulation technique; Ref. 4 contains a derivation for the MIMO case. This technique assumes that the plant model in the simulation exactly emulates the actual HST plant. Subject to this assumption, the simulation allows comparison of the performance of a redesigned controller to that of the in-flight controller under the application of an identical set of disturbance inputs.

The nonlinear simulation includes the 0.8 N-m torque limits of the RWA units and appears to account for some fixed-point arithmetic effects by including the software limiters of the DF-224 flight computer. The modifications made to the nonlinear simulation, along with the reasoning behind them, are as follows:

1) The simulation was modified to run on a more powerful platform. This reduced execution time by roughly a factor of 6.

2) The original simulation is hard coded such that the controllers must be in the form of the existing HST flight controllers, rendering it of little use in the study of controllers that are anything more than slight changes to the existing PID and SAGA flight controllers. The modified simulation implements controllers as state-space realizations, so any controller may be evaluated, regardless of its structure.

3) The original simulation apparently uses software limiters to simulate the effects of fixed-point arithmetic, and the limiters appear to be peculiar to the implementation of the existing flight controllers. Since the controllers in the modified simulation are state-space

realizations, a new and more general fixed-point arithmetic simulation is included.

An emulation of fixed-point arithmetic effects is included in the modified HST nonlinear simulation in order to investigate the performance of redesigned controllers in the face of the fixed-point arithmetic implementation of the DF-224 flight computer. The DF-224 inherently represents numbers as integers, but it appears the user is free to assume a radix point anywhere in the binary word. The modified simulation includes code to take into consideration three sources of error caused by fixed-point calculations:

1) The coefficients of the desired digital signal processing algorithm may not be exactly representable by the fixed-point computer.

2) Any inputs or outputs of the system may not be converted precisely due to the finite word lengths of the A/Ds and D/As.

3) Any arithmetic operations (e.g., additions or multiplications) are subject to quantization to the nearest representable result.

The actual fixed-point calculations are performed as a two-step process in which the number is first converted to an equivalent integer representation of the fixed-point number by means of

$$N(X) = \mathrm{IP}[X \cdot 2^p + r\,\mathrm{sgn}(X)] \tag{1}$$

In Eq. (1), $N(X)$ is the resultant integer, IP[·] is the integer part operator, X is the number to be operated on, p is the desired number of binary places to the right of the radix point, r is the designation for rounding or truncation (0 for truncation and 0.5 for rounding), and sgn is the sign operator. Following this conversion to integer format, the number is compared to the largest number representable with the given word length and radix position. The calculation of this maximum allowable value is accomplished as

$$Z = 2^i - 1 \tag{2}$$

where Z represents the maximum number and i represents the number of bits in a single fixed-point word. Finally, a return to decimal representation is accomplished by means of

$$D(X) = \frac{X}{2^p} \tag{3}$$

In Eq. (3), $D(X)$ represents the resultant decimal number, X is the number operated upon, and p is the number of binary places to the right of the radix point.

Modifications to the subroutines corresponding to the controller simulations were required in order to implement fixed-point arithmetic for the digital controller calculations. The modifications are to quantize 1) each controller coefficient, 2) the controller inputs, and 3) any controller calculations. Since the controllers are implemented as state equations in the simulation, the coefficient quantization is a simple matter of quantizing each element of the A, B, C, and D matrices. The quantization of the input vectors follows in a similar fashion. The final controller quantization involves quantizing the calculations that determine the next states and the current outputs from the present states. Although it has not been possible to ascertain the precise details of the DF-224 controller algorithm, the fixed-point implementation in the modified simulation provides the only available means to investigate the effects of fixed-point arithmetic on the performance of the redesigned controllers. It is also important to note that, once the structure of the algorithm in the DF-224 is known, these details can be emulated by a judicious choice of the state-space realizations of the controllers. The experience of the authors is that emulating the structure of the control processor algorithms is critical; i.e., the closed-loop performance of a controller implemented in fixed-point arithmetic can be highly sensitive to the algorithm structure.[5]

The simulations are employed to compare redesigned controllers to the SAGA-II controller; i.e., SAGA-II is the baseline controller against which all others are compared. Since this is the case, the available sets of simulation input data were examined to see which set exhibited the largest LOS errors when simulating the SAGA-II controller. Simulating redesigned controllers with such data would provide an indication of their worst-case performance. All simulations were subsequently performed using the 90 deg flight data, since it appears to be the worst-case available data.

Since there are two MIMO plant models available, the models were examined to determine which is the better model for simulation purposes. The TREETOPS models are those used by NASA in simulations to evaluate controller performance, whereas the composite SISO modal models were those used for design of the existing PID and SAGA-II flight controllers. However, in the redesign effort, the H_∞ design is based on the MIMO modal plant model, but the controller obtained via numerical techniques is based on the TREETOPS models. It was decided that all simulations of the redesigned controllers would be performed with both the TREETOPS-based models and the MIMO modal model in order to obtain a thorough evaluation of controller performance.

H_∞ Controller Design

The H_∞ controller design is a MIMO loop-shaping approach that yields a controller that satisfies desired performance and robustness specifications. The HST PCS redesign problem provides an excellent opportunity to apply H_∞ design techniques to an existing complex MIMO system. Such an exercise allows the comparison of H_∞ controller design to other design methods and yields an indication of the practicality of using H_∞ techniques on complex realistic systems. The authors have previously applied analytical H_∞ design techniques to several problems.[2,6] In referring to the HST PCS, the term *plant* and the notation G_p in subsequent discussions refer to the Fig. 1 blocks $T_{W/V}$, $T_{V/G}$ and all components between them.

As stated previously, the redesign philosophy is to obtain high controller gain in the frequency range of the dominant disturbances, thereby accomplishing some degree of disturbance rejection. The loop-shaping approach of H_∞ controller design theory is ideally suited to achieving this type of specification. In using H_∞ design algorithms, frequency-dependent weighting functions are applied to certain outputs of the control system; these weighting functions specify the desired system performance and robustness.

Figure 4 shows the block diagram used to set up a typical H_∞ design problem. The weighting function W_1 is applied to the error signal, and if this signal is denoted as E, it is apparent that $E = SU$, where $S = (I + G_pG_c)^{-1}$, which is commonly known as the sensitivity function. If the plant output is denoted as V, it is clear that W_3 weights the function $V = TU$, where $T = (I + G_pG_c)^{-1}G_pG_c$, which is known as the complementary sensitivity function. The use of W_1 and W_3 is referred to as the mixed-sensitivity approach to H_∞ design. Once W_1 and W_3 are specified, the H_∞ design algorithm determines whether an internally stabilizing controller exists that satisfies the constraints that 1) the frequency-dependent singular values of the sensitivity function lie below the inverse of the W_1 weighting function and 2) the singular values of the complementary sensitivity function lie below the inverse of the W_3 weighting function. If no stabilizing controller exists that satisfies these constraints, the constraints must be relaxed until an acceptable controller is found. The reader interested in further details of H_∞ design philosophy and algorithms is referred to Refs. 7–9 and the references therein.

If a disturbance input is introduced into Fig. 4 between the controller and the plant, the equation for the disturbance contribution to the output is $V = (I + G_pG_c)^{-1}$, G_pT_d, or $V = SG_pT_d$, where $S = (I + G_pG_c)^{-1}$, the sensitivity function previously described, and V is the plant output. Since the controller can be designed for sensitivity function attenuation in the disturbance frequency range, it is easy to see how sensitivity function design can provide disturbance rejection in the system output. On the other hand, providing attenuation of the complementary sensitivity function provides robustness to model uncertainty in the frequency range of the attenuation. It should be noted that attenuation of either sensitivity or

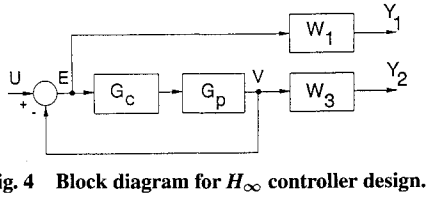

Fig. 4 Block diagram for H_∞ controller design.

complementary sensitivity may be achievable in a given frequency range, but not both. The approach to the HST redesign is to 1) achieve sensitivity function attenuation in the low-frequency ranges where the SA disturbances are known to exist, thereby reducing the effects of the disturbances, and 2) achieve as much robustness to model uncertainty as possible while meeting the disturbance attenuation specifications.

The HST controller must contain an integrator in each axis in order to retain the number of free integrators required to eliminate steady-state errors caused by gravity gradients and aerodynamic forces. Constructing the controller as a PID controller in cascade with the H_∞ controller meets this constraint.

Initial design attempts failed to yield stabilizing controllers due to numerical difficulties encountered by the H_∞ algorithms. After considerable analysis, it was decided the problems were most likely caused by the large number of PID integrator poles and rigid-body mode poles clustered at the origin of the w plane. A constant prefeedback was applied to the plant, as seen by the H_∞ controller, to decluster these poles and move the rigid-body modes off of the imaginary axis. The prefeedback is selected such that the rigid-body poles are moved off of the imaginary axis, but no poles are moved so far into the right-half plane that they cannot be stabilized. Furthermore, selection of prefeedback gains greater than unity effectively increases the gain of the PID controller, increasing loop gains at low frequencies. The H_∞ controller must then stabilize the system that contains the prefeedback and provide the specifications indicated by the weighting functions. Once an H_∞ controller is obtained, the prefeedback is included as a feedforward path in parallel with the H_∞ controller; i.e., the prefeedback can be thought of as a direct feedthrough component of the H_∞ controller. Thus, in the final implementation, the prefeedback does not wrap around the PID controller, so it causes no reduction in the low-frequency gain of the system. As a result, the system type is maintained.

Figure 5 illustrates the block diagram of the problem setup for input to the H_∞ algorithm with prefeedback K_f in place. The modified plant, consisting of the blocks G_p, PID, -1, and K_f, was built in the z plane based on the 90 deg MIMO modal plant model and then converted to a w-plane realization, since the H_∞ design algorithms must be applied to continuous-time models. Figure 6 displays the w-plane weighting functions used in designing the controller. The term W_1 is a sixth-order weighting function comprised of identical second-order weightings applied to each of the three PCS loops. This weighting specifies 14 dB of sensitivity function attenuation in the w-plane frequency range of 0.001–0.1 Hz. The term W_3, a third-order weighting comprised of identical first-order weightings applied to each plant output, specifies complementary sensitivity function attenuation (hence robustness to model uncertainty) at w-plane frequencies above 100 Hz.

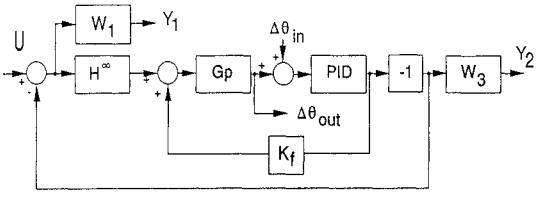

Fig. 5 The H_∞ problem setup with prefeedback.

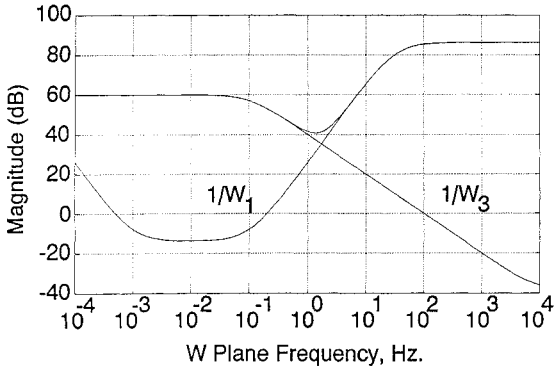

Fig. 6 Weighting functions for H_∞ design.

The design algorithms were used to obtain an 82nd-order H_∞ controller that meets the specifications. The design is successful in the sense that, under linear analysis and simulation, it stabilizes the MIMO modal plant model and provides improved disturbance attenuation over the SAGA-II controller implementation. The controller was inserted into the PCS loop and compared with the SAGA-II implementation via frequency-domain analysis and time-domain simulation.

The disturbance rejection achieved with the H_∞ controller is superior to that of SAGA-II in all three vehicle axes. As a typical example, the V_3 axis disturbance to output frequency response of the HST PCS with the H_∞ controller has up to 20 dB greater attenuation of disturbances than the SAGA-II case at all frequencies below 2 Hz, but at frequencies above 2 Hz the attenuation is greater for SAGA-II. Thus, the design goal of increased low-frequency disturbance attenuation was attained. Similar results were achieved in the other two axes.

The results of a linear simulation of the system with the MIMO modal model and H_∞ controller for the V_3 LOS are presented in Fig. 7. Figure 8 shows the results of the same simulation with the SAGA-II controller. Table 1 contains a numerical comparison of the simulated LOS data of the two controllers based on a linear simulation using 500 s of on-orbit data input data that includes a day-to-night terminator.

Table 1 Linear simulation LOS attitude with MIMO modal model

	Peak value, marc-s		Root-mean-square value, marc-s	
Axis	SAGA-II	H_∞	SAGA-II	H_∞
V_1	136.8	70.2	26.4	9.71
V_2	28.9	12.3	3.44	2.44
V_3	67.8	48.3	2.44	4.63

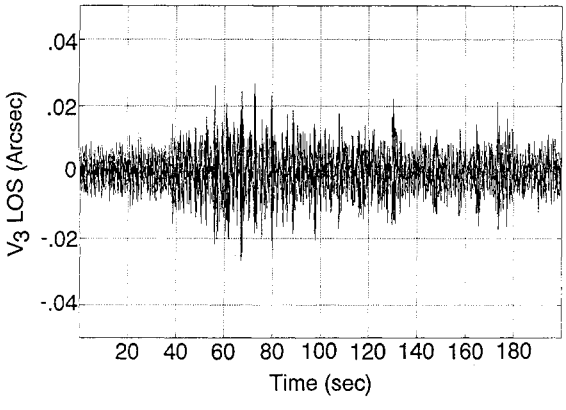

Fig. 7 Simulated V_3 LOS with H_∞ controller.

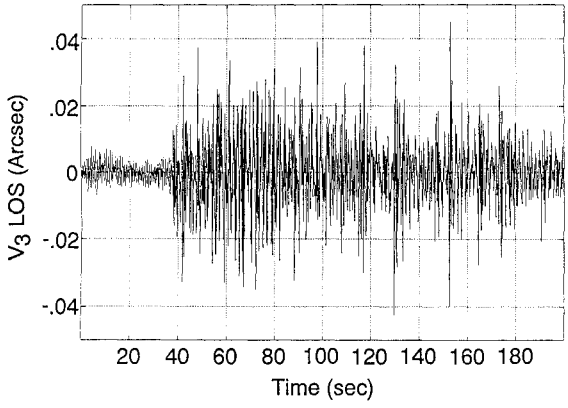

Fig. 8 Simulated V_3 LOS with SAGA-II controller.

Power spectral density estimates obtained from the V_3 LOS information reveal that the H_∞ controller reduces the magnitude of the V_3 LOS PSD in the low-frequency ranges but increases it in the higher frequencies. This is as expected, since the disturbance to output magnitude frequency responses discussed in preceding paragraphs indicate that the H_∞ controller causes greater low-frequency attenuation but less attenuation in the high frequencies than the SAGA-II case. In the case of the HST PCS, this results in improved performance since the SA disturbances occur at low frequencies. Again, similar results were obtained in the other two axes. Clearly, these results show that broadband low-frequency disturbance attenuation proves effective in reducing the disturbance effects.

A simulation with torque limits in place was performed, with the result that the inclusion of torque limits destabilizes the system. In light of the this fact, any further H_∞ design efforts should include specifications that limit available control energy. In order to test the robustness of the controller to changes in the plant model, a linear simulation was performed using a 90 deg TREETOPS plant model rather than the MIMO modal plant model, with the result that again the system proved to be unstable. It was subsequently found that under linear simulation the H_∞ controller does not stabilize any available HST model except the MIMO modal plant model for which it was designed.

Reduction techniques were applied to the H_∞ controller in an attempt to reduce the order. Regardless of order, none of the resulting controllers stabilize the MIMO modal plant model or any other available HST plant model. All simulation attempts with these reduced-order controllers indicate instability.

Obtaining a successful H_∞ controller for the HST PCS was a difficult and time-consuming process. An 82nd-order H_∞ controller was developed that provides superior linear simulation performance to the SAGA-II controller with the MIMO modal plant model, but it destabilizes the system when torque limits are included or when any HST plant model other than the design model are used as the simulation plant. Furthermore, reduced-order versions of the H_∞ controller fail to stabilize any available HST plant model. Despite the fact that a controller was designed that improves over the SAGA-II controller in some respects, the H_∞ controller would not yield satisfactory performance in the HST. Clearly, applying H_∞ design techniques to a system as complex as the HST is far from being a straighforward process. Any further H_∞ design efforts should include specifications to limit controller energy in order to account for the reaction wheel torque limits.

Numerical Redesign

In order to achieve H_∞-type closed-loop specifications and to obtain a controller of an acceptable order, an iterative numerical method was employed for design. This method, which is similar to multiple-objective optimization, has been previously used to aid in the design of an effective controller for a large space structure ground test facility at NASA Marshall Space Flight Center.[10] A few of the advantages of this method over analytical techniques include 1) the capability of using frequency response estimates of the plant generated either from experimental data or from an analytical model, 2) the ability to have some measure of control over the structure (e.g., decentralized) and order of the controller, and 3) the capability of simultaneously specifying several closed-loop design constraints. The primary drawbacks to this approach are that the user must specify an initial, stabilizing controller and that conditions for constraint feasibility are often very difficult to obtain. The development of the Model and Data-Oriented Computer-Aided Design System (MADCADS), an interactive software system that uses this numerical method, is currently underway at Ohio University with support provided by NASA Marshall Space Flight Center. The reader interested in details of the MADCADS algorithms is advised to consult Ref. 11.

The numerical redesign is based on the SAGA-II controller. Each of the diagonal terms of SAGA-II consists of second-order PID compensation for rejection of low-frequency torque disturbances, finite impulse response (FIR) filters for suppression RWA isolator modes, and lightly damped poles near 0.1 and 0.6 Hz to help suppress the effect of the disturbances generated by SA motion. All of the off-diagonal terms of the controller are zero. General frequency-domain performance properties of the PCS using SAGA-II are illustrated by the magnitude frequency response of the closed-loop transfer function (generated with the TREETOPS model) from the disturbance input to the measured LOS of the V_3 axis given in Fig. 9. This response reveals the deep but narrow notch at 0.1 Hz that is the result of the lightly damped controller pole that is intended to reduce the impact of the out-of-plane bending of the SAs on the LOS. The notch at 0.6 Hz, which suppresses the effect of in-plane SA bending, is also apparent. The most important observation is the fact that there are several frequency regimes in which the level of disturbance rejection is not nearly as pronounced as it is at 0.1 and 0.6 Hz. As is to be shown, the overall level of disturbance suppression can be improved by increasing the damping ratios of the controller poles that produce these notches.

MIMO stability robustness of the system, as measured by a peak value of 12 dB in the complementary sensitivity function (a measure of unstructured multiplicative output uncertainty in the plant), is rather poor. The classical SISO stability margins given in Table 2 also indicate poor stability robustness.

A 500-s linear simulation of the closed-loop system using SAGA-II and the MIMO modal plant model was performed. The PSD estimate of the V_3 axis response is given in Fig. 10. It is important to recognize that although this PSD does indicate concentrations of power density near 0.6 Hz, there are also significant levels of power

Table 2 SISO gain (GM) and phase (PM) margins with TREETOPS plant and SAGA-II controller

Axis	PM	Lower GM, dB	Upper GM, dB
V_1	25 deg	15	10
V_2	15 deg	20	5
V_3	15 deg	25	7

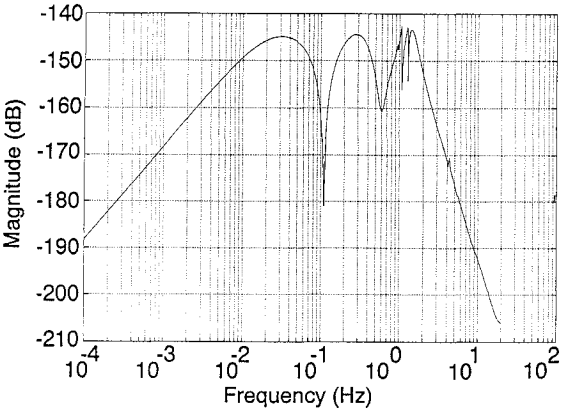

Fig. 9 The V_3 disturbance to LOS output magnitude response with SAGA-II controller.

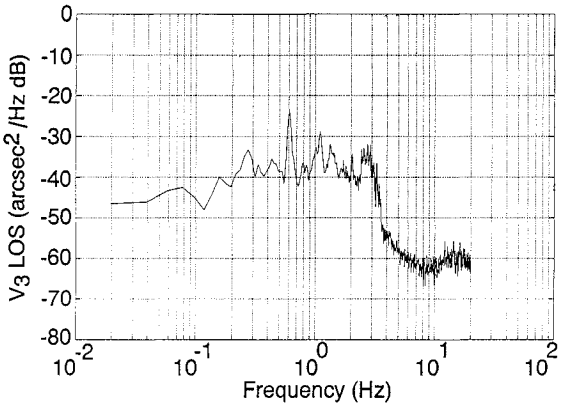

Fig. 10 Linear simulation V_3 LOS PSD estimate with SAGA-II controller.

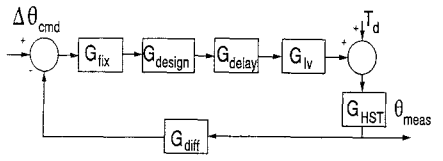

Fig. 11 Block diagram for numerical design.

density at nearby frequencies. PSD estimates of the V_1 and V_2 axes reveal similar properties.

The block diagram shown in Fig. 11 was chosen as the basis for the numerical design process. The signals (z domain) and blocks in the figure are defined in the Nomenclature section. From this diagram, measured attitude as a function of the disturbance torque is calculated to be $\theta_{\text{meas}} = S_\theta G_{\text{HST}} T_d$, where $S_\theta = (I + G_{\text{HST}} G_{Iv} G_{\text{delay}} G_{\text{design}} G_{\text{fix}} G_{\text{diff}})^{-1}$ is the output sensitivity function.

Since it is desirable to reduce the impact of T_d on θ_{meas}, it is necessary to keep $S_\theta G_{\text{HST}}$ small in norm at frequencies where T_d contains significant power. This can be achieved by designing the controller such that S_θ is small in norm at the appropriate frequencies. It is also desirable to keep the complementary sensitivity function $T_\theta = I - S_\theta$ small in norm at frequencies for which the model of the plant is suspected to be inaccurate (primarily high frequencies).

The modifications to SAGA-II are now described. Analysis of the geometry of the HST indicates that, regardless of SA orientation, any in-plane bending of the SAs has only a minor impact on HST motion about the V_2 axis. Therefore, the lightly damped pole located at 0.6 Hz in the V_2 axis of the SAGA-II controller was eliminated. This allowed for an increase in gain in this loop while maintaining closed-loop stability. Since in-plane bending has a significant impact on the V_1 and V_3 axes (the degree depending on the particular SA orientation), and since the out-of-plane SA bending has an impact upon all HST axes, especially V_2, the frequencies of the other poles of SAGA-II were not changed. However, the damping ratios of these poles were increased in order to spread the disturbance rejection benefits that they offer over a broader range of frequencies. This change was based upon the fact that the PSD estimates from the simulation with SAGA-II reveal that the disturbance power density is not simply isolated to the frequencies near 0.1 and 0.6 Hz but is also present in significant levels at nearby frequencies. A final change was the inclusion of two stages of phase lead compensation in each of the primary axes of the controller in order to improve the stability robustness characteristics of the system. The high-frequency FIR filters that have been used to suppress RWA isolator modes and the PID compensation were left intact.

To set up the numerical redesign, the frequency response of the HST was generated from 10^{-4} to 20 Hz using the TREETOPS model of the 90 deg SA orientation (the only MIMO model available at the time of the numerical redesign). Frequency responses were also generated for the fixed stage of compensation (PID, disturbance suppression poles, and FIR filters). These responses were used as input to MADCADS along with the initial values for matrices corresponding to a state model of the sixth-order phase lead stages, which constitute the free part of the controller. Frequency-domain design constraints on the sensitivity function (for disturbance rejection) and complementary sensitivity function (for stability robustness) were also used as input to MADCADS. The constraints on S_θ and T_θ were chosen in such a way as to attempt to maintain the disturbance attenuation of the initial controller with the objective of improving the stability robustness, especially at frequencies above 1.0 Hz.

The MADCADS program yielded a 28th-order controller that provided comparable performance and improved stability robustness over the initial controller. Final results and design constraints are given in Figs. 12 and 13. It is suspected that the inability to fully satisfy the design constraints is due to the fact that the free part of the controller design is only sixth order and that the constraints were in constant competition; i.e., the only way to improve the stability robustness is to weaken the disturbance rejection constraint.

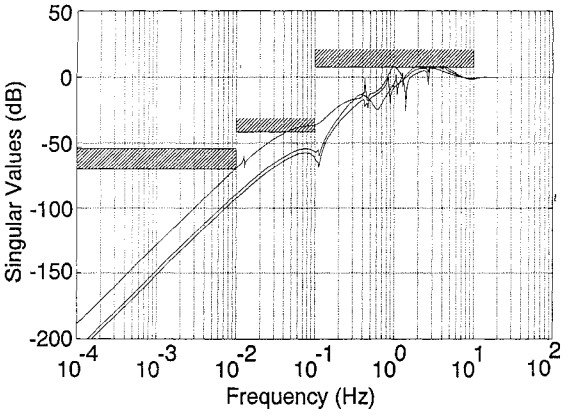

Fig. 12 Sensitivity function singular values with MADCADS controller.

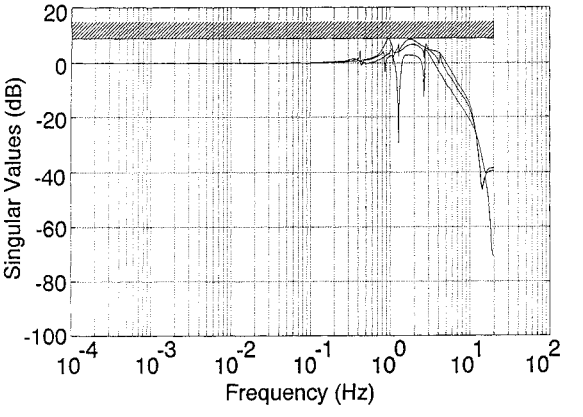

Fig. 13 Complementary sensitivity function singular values with MADCADS controller.

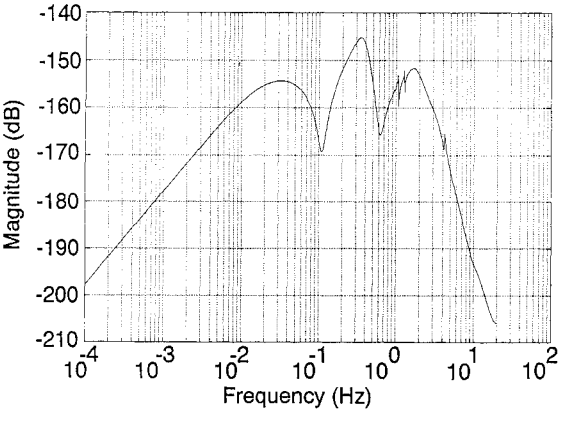

Fig. 14 The V_3 disturbance to LOS output magnitude response with MADCADS controller.

Classical SISO stability robustness measures are given in Table 3. When compared to results obtained with SAGA-II (Table 2), however, these results reveal significant improvements in the stability robustness characteristics of the system.

The V_3 axis closed-loop magnitude frequency response (generated using TREETOPS model) of the disturbance input to the LOS output transfer function with the MADCADS controller is shown in Fig. 14. Comparison of this plot with that given in Fig. 9 indicates considerable improvement in disturbance rejection over that achieved by SAGA-II.

Simulations with and without reaction wheel torque limits (0.8 N-m) were performed with the MADCADS controller in the loop. The PSD estimate of the V_3 axis response from the linear simulation (no torque limits) using the MIMO modal model is shown in Fig. 15. Comparing this PSD estimate with that obtained using SAGA-II

Table 3 SISO gain and phase margins with TREETOPS plant and MADCADS controller

Axis	PM	Lower GM,dB	Upper GM,dB
V_1	30 deg	50	7
V_2	40 deg	15	7
V_3	30 deg	20	7

Table 4 Linear simulation LOS Attitude with MIMO modal model

	Peak value, marc-s		Root-mean-square value, marc-s	
Axis	SAGA-II	MADCADS	SAGA-II	MADCADS
V_1	136.8	114.8	26.4	21.1
V_2	28.9	18.9	3.44	2.33
V_3	67.8	57.8	2.44	5.03

Table 5 Linear simulation LOS attitude with TREETOPS model

	Peak value, marc-s		Root-mean-square value, marc-s	
Axis	SAGA-II	MADCADS	SAGA-II	MADCADS
V_1	170.9	100.9	32.4	23.1
V_2	28.9	17.4	3.36	2.25
V_3	68.0	61.0	7.11	5.27

Table 6 Torque limit simulation LOS attitude with MIMO modal model

	Peak value, marc-s		Root-mean-square value, marc-s	
Axis	SAGA-II	MADCADS	SAGA-II	MADCADS
V_1	136.3	153.7	26.6	21.5
V_2	28.8	25.2	3.44	2.60
V_3	75.7	76.2	6.75	5.54

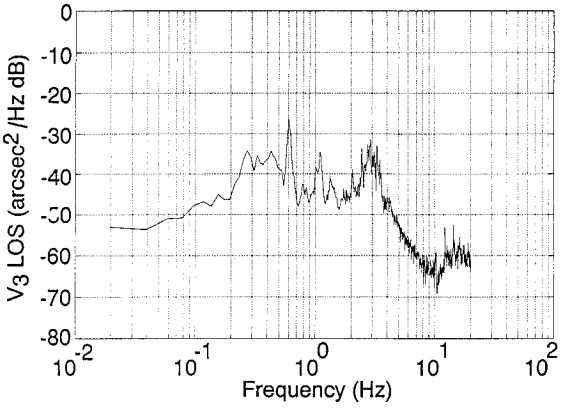

Fig. 15 Linear simulation V_3 LOS PSD estimate with MADCADS controller.

reveals that increased disturbance rejection is achieved at nearly all frequencies. Peak and root-mean-square (rms) results using the non-composite MIMO modal model and TREETOPS model are given in Tables 4–7. In the large majority of cases the MADCADS controller proves to have better peak and rms performance than SAGA-II, especially in simulations using the TREETOPS model. These general performance improvements can be attributed to the increased disturbance rejection at nearly all frequencies of interest, as is illustrated by Fig. 14.

Another simulation including reaction wheel torque limits and the fixed-point arithmetic implementation was performed using the MADCADS controller. Tabular data are provided for a simulation using MIMO modal model and a simulation using the TREETOPS model in Tables 8 and 9, respectively. These data clearly illustrate that performance degradations occur with the simulation of fixed-point arithmetic, evidenced especially in the peak values using the TREETOPS model. It is important to realize that these simulations are for a rather arbitrary controller state-space realization and that different realizations can produce widely varying simulation results. Therefore, these simulations do not necessarily reflect the performance of an onboard implementation. More accurate simulations would require more specific information regarding the HST control computer algorithms.

Table 7 Torque limit simulation LOS attitude with TREETOPS model

	Peak value, marc-s		Root-mean-square value, marc-s	
Axis	SAGA-II	MADCADS	SAGA-II	MADCADS
V_1	171.5	123.9	32.5	23.9
V_2	28.9	20.9	3.40	2.48
V_3	74.2	70.4	7.34	5.67

Table 8 Simulated LOS attitude with torque limits and fixed-point arithmetic using MADCADS controller and MIMO modal model

Axis	Peak, marc-s	Root-mean-square, marc-s
V_1	198.0	47.8
V_2	27.2	3.62
V_3	110.0	10.8

Table 9 Simulated LOS attitude with torque limits and fixed-point arithmetic using MADCADS controller and TREETOPS model

Axis	Peak, marc-s	Root-mean-square, marc-s
V_1	440.8	45.1
V_2	43.8	3.36
V_3	132.9	8.80

Summary and Conclusions

Efforts in redesigning the controller for the HST PCS to achieve improved performance in the face of SA induced disturbances have been presented. Controller design via standard analytical H_∞ techniques led to a successful 82nd-order controller that provides marked improvement in linear simulation results over those obtained using SAGA-II; however, it results in an unstable response when RWA torque limits are included or when a plant model other than the design model is used for simulation. Reduced-order controller versions of the H_∞ controller obtained through model reduction techniques also result in an unstable closed-loop system. The torque limit results suggest that any subsequent H_∞ design efforts should include specifications to limit controller energy to take into account these limits. Clearly, H_∞ controller design applied to the HST is not a straightforward process.

A successful 28th-order controller that provides simulation performance superior to that of SAGA-II was designed via an iterative numerical technique. Although some of the stated performance goals were not achieved, the redesigned controller performance is significantly improved over that of SAGA-II when run with identical simulations. This controller performs well when a plant model other than the design model is used and when reaction wheel torque limits are included. A key reason for the success of this controller is the broadband disturbance rejection characteristics of the closed-loop system. SAGA-II, on the other hand, places a greater emphasis on narrow-band attenuation at 0.1 and 0.6 Hz at the expense of attenuation of disturbances at other frequencies.

Another area in which significant work was performed was modification of the NASA simulation software. The controller implementations in the simulation have been changed from the hard-coded PID and SAGA-II flight controllers to general state-space realizations, allowing the use of any controller in the simulation. Torque limits and a general fixed-point arithmetic simulation have also been included.

Acknowledgments

The HST redesign was supported by NASA Marshall Space Flight Center under Grant NAG8-242 and was made possible by the personnel of the Pointing Control Systems Branch.

References

[1]Sharkey, J. P., Nurre, G. S., Beals, G. A., and Nelson, J. D., "A Chronology of the On-Orbit Pointing Control System Changes on the Hubble Space Telescope and Associated Improvements," *Proceedings of the AIAA Guidance, Navigation, and Control Conference* (Hilton Head, SC), AIAA, Washington, DC, 1992, pp. 2–15.

[2]Irwin, R. D., Frazier, W. G., and Medina, E., "Controller Design for Large Flexible Aerospace Structures via Numerical Techniques for Achieving Multi-Objective Design Specifications," NASA NAG8-123, June 1992.

[3]Sills, J. W., Jr., "HST On-Orbit Structural Dynamics Models and Modal Gain Factors of October 1991," Lockheed Engineering, Memorandum SPS-657, Sunnyvale, CA, Nov. 1991.

[4]Irwin, R. D., Glenn, R. D., Frazier, W. G., Lawrence, D. A., and Follett, R. F., "Controller Redesign for the Hubble Space Telescope," NASA NAG8-242, Sept. 1993.

[5]Follett, R. F., "Emulation and Characterization of Digital Controllers Realized with Fixed Point Arithmetic," M. S. Thesis, Mississippi State Univ., Mississippi State, MS, May 1984.

[6]King, J. A., and Irwin, R. D., "Issues in the Application of H_∞ to Large Space Structures," paper presented at 22nd Southeastern Symposium on System Theory, Cookeville, TN, March 1990.

[7]Maciejowski, J. M., *Multivariable Feedback Design*, 1st ed., Addison–Wesley, Wokingham, England, 1989.

[8]Glover, K., "All Optimal Hankel-Norm Approximations of Linear Multivariable Systems and their L-Infinity Error Bounds," *International Journal of Control*, Vol. 39, No. 6, 1984, pp. 1115–1193.

[9]Chiang, R. Y., and Safanov, M. G., *MATLAB Robust Control Toolbox User's Guide*, 1st ed., Mathworks, South Natick, MA, 1988.

[10]Frazier, W. G., and Irwin, R. D., "Designing Reduced-Order Linear Multivariable Controllers Using Experimentally Derived Plant Data," *Journal of Guidance, Control, and Dynamics*, Vol. 16, No. 1, 1993, pp. 53–58.

[11]Frazier, W. G., "Search-Based Methods for Computer-Aided Controller Design Improvement," Ph.D. Dissertation, Ohio Univ., Athens, OH, June 1993.